Production Engineering
https://doi.org/10.1007/s11740-020-00980-x

PRODUCTION PROCESS

Analytical force modelling for micro milling additively fabricated Inconel 625

Andrea Abeni[1] · Dario Loda[1,2] · Tuğrul Özel[2] · Aldo Attanasio[1]

Received: 24 April 2020 / Accepted: 1 September 2020

Abstract
In recent years, miniaturization of components has been concerned with several industrial fields including aerospace, energy, and electronics. This phenomenon resulted in increasing demand of micro-components with complex shape and high strength, often in high-temperature environment. Nickel-based superalloys such as Inconel 625 are a class of material suitable to aforementioned applications and can be successfully processed with Additive Manufacturing (AM). Moreover, micro-milling can be employed to manufacture micro-scale features on the additively fabricated parts or to achieve better surface finishes, as required for high-precision mechanical assemblies. In micro machining, it is possible to notice a lack of scientific study focusses on the material removal behavior of difficulty-to-cut alloys produced via Additive Manufacturing. This paper describes an analytical cutting force model suitable also for AM'd parts which considers the presence of ploughing- and shearing- dominated cutting regimes. A refinement procedure of the cutting force model was defined and applied by performing an experimental work on Inconel 625 samples fabricated by LaserCUSING™. A search algorithm was employed to develop an iterative methodology to determine the unknown cutting force model parameters. The model was successfully utilized to predict how the cutting force is affected as the process parameters change.

Keywords Micro milling · Cutting force model · Nickel-based superalloy · Minimum cutting thickness · Selective laser melting

1 Introduction

Additive manufacturing (AM) is a collection of layer-by-layer building processes which can be successfully employed using polymers, ceramics and metals. The type and the aggregate state of the feedstock material as well as the binding mechanism between the overlapped layers must be considered for an AM classification [1]. In AM of metals, the feedstock material is usually provided in the form of powder and an energy source produces the localized melting. It is followed by the subsequent solidification of the added material over the substrate in the form of layers, with a typical thickness ranging between 20 and 150 µm [2, 3]. The most common Additive Manufacturing processes for powder metals are powder bed fusion (PBF) type which includes laser powder bed fusion (L-PBF) and electron beam powder bed fusion (EB-PBF). Furthermore, L-PBF processes are also known with their commercial names such as Selective Laser Melting (SLM), Direct Metal Laser Sintering (DMLS™), LaserCUSING™ and Laser Metal Fusion (LMF). Standard L-PBF AM processes allow obtaining fully dense parts by locally melting a thin layer of metal powder. The energy source is a high-power focused laser beam [4]. In each layer, the laser spot is first focused with f-theta lenses and then moved within the cross section of the part by means of numerically controlled mirrors (galvanometer scanners), following a path defined by the scan pattern. The possibility to fabricate very complex shapes from difficult-to-cut materials and to avoid fixturing and work holding assembly phase and to limit the material waste and scraps are just some of the established AM advantages [5]. Nowadays L-PBF (or SLM) processes are rapidly spreading throughout the industrial manufacturing finding applications in several branches, such as aerospace and biomedical industries. Moreover, the final

✉ Aldo Attanasio
aldo.attanasio@unibs.it

[1] Department of Mechanical and Industrial Engineering, University of Brescia, V. Branze 38, 25123 Brescia, Italy

[2] Manufacturing and Automation Research Laboratory, Industrial and Systems Engineering, Rutgers University, Piscataway, NJ, USA

Published online: 08 September 2020

product quality is not comparable with the standards achievable through the conventional subtractive material removal methods. The main drawback of additively manufactured components in metals is the inferior quality of the surface finish and high surface roughness [6], therefore further post-process surface treatments are usually required to finish and to refine the surfaces of the build product.

Micro machining can be defined as machining performed with tools with a cutting edge radius comparable to the undeformed chip thickness or the depth of cut. Micro machining has already become a widespread manufacturing process for the fabrication of small features on metallic components [7]. Several applications of micro machining operations can be found in electronics and opto-electronics, biomedical, automotive, aerospace and energy industries [8]. The high removal rates, low material waste and elevated accuracy of micro machining guarantee economic efficiency and high flexibility. Among the micro machining processes, the micro milling is certainly one of the most flexible processes for achieving high productivity and being suitable for widespread applications among manufacturing industries. The advantages of micro milling are strongly related to the small size of the cutting tools, which typically have a diameter smaller than 1 mm and can be as small as few hundred micrometers with a cutting edge roundness usually in the order of a few micrometers [9].

Nickel-based superalloys (Ni–Cr, Ni–Co–Cr, Ni–Fe–Cr, or Ni–Co–Fe type) are some of the metal alloys which can be utilized in AM processes in the powder form. Such materials are widely used in aerospace and power industries, as well as in biomedical industry, due to their high strength, high temperature resistance, super-elasticity behavior and good properties in terms of bioactivity [10]. The trademark name "Inconel" commonly identifies a specific class of Nickel–Chromium alloys with superior mechanical proprieties, such as high resistance to corrosion and temperature [11]. Moreover, Inconel superalloys are known to be very difficult-to-cut [12] due to their ability to retain their very high yield strength and the low thermal conductivity. The Inconel superalloy proprieties and difficulty in workability make these alloys more suitable for the integration between the metal AM and the conventional subtractive material removal processes. Complex-shaped and miniaturized parts could be built via metal AM methods and subsequently their surfaces could be finished or polished through micro milling operations [13].

The micro machining of difficult-to-cut metal alloys shows some unique characteristics because of the conventional miniaturization technique. These characteristics include size effect, burr formation, rapid tool wear, higher than expected cutting forces and tool run-out which are the most common micro milling related issues [9, 14, 15]. At this scale, the depth of cut or undeformed chip thickness should be compared to the tool edge radius size. Therefore, the material removal mechanism is strongly affected by the negative tool rake angle, since the chip does not form unless the cutting thickness is greater than a critical value named minimum uncut chip thickness (MUCT). If the uncut chip thickness is lower than the MUCT, the cutting process is characterized by combined effects of elastic and plastic deformations of the material known as ploughing [16, 17]. The minimum chip thickness effect and the related elastic recovery of the cut material causes high or fluctuating cutting forces and poor surface roughness especially at low feed rates. Several researchers demonstrated that usually the minimum uncut chip thickness ranges between 1/4 and 1/3 of the tool cutting edge radius [18–20]. It was recognized that the MUCT identification is a crucial procedure to determine the appropriate feed rate and consequently the feasible machinability parameters for the work materials.

The experimental investigation in the context of micro milling must be conducted with specific and expensive laboratory equipment. It is necessary to measure process outcomes such as tool run-out, cutting forces, and tool wear rate directly. Therefore, machining models are powerful tools to investigate all of the aforementioned phenomena, without conducting experiments in each possible cutting condition. Models must be formulated correctly and calibrated by comparing their prediction with the results of appropriate machining tests. A reliable model should consider the ploughing effect in the cutting force computation since it possesses a significant influence on the force magnitude. Several analytical models are currently available for micro milling [21–23], but only a small number of them considers both the cutting regime effects (i.e. ploughing and shearing). In addition, the investigation of ploughing effects in micro machining process for work materials fabricated via AM has not been studied before.

The main objective of this work is to investigate the machinability of a specific Ni–Cr–Mo superalloy, Inconel 625, a superalloy characterized by high temperature resistance, high corrosion resistance, and good wear resistance properties [24]. Micro milling experimental tests were performed on an additively manufactured workpiece obtained via SLM. The experimental tests were designed with the specific purpose of operating micro machining under orthogonal cutting condition. The 2D cutting configuration facilitated the modeling of the process, which allowed a deeper investigation of the chip formation mechanism. An analytical force model was developed and subsequently optimized through the Particle Swarm Optimization (PSO) technique [25] for Inconel 625. The analytical force model predicts the cutting force by considering the concomitant presence of two different deformation regimes, the ploughing and the shearing, and it can be calibrated also for material fabricated by conventional process.

2 Mechanistic modelling for micro milling

Nowadays, in the industrial landscape, the necessity to develop reliable machining models is rapidly growing. The machining process modelling can be applied in several contexts, as the monitoring systems and the adaptive control. A considerable number of models have been developed in machining field in the last five decades by considering different cutting conditions, process parameters, and materials properties. In any case, a machining analytical force model computes cutting forces as a function of cutting parameters and tool geometry. A reliable force model can be used to predict the maximum cutting forces before the execution of machining operations, in order to assess if the tool will undergo excessive stresses. Besides this, the force model can be used for the generation of reference force data usable for the comparison with finite element method (FEM) predictions. This approach allows to refine finite element (FE) simulations by using the analytical model prediction as benchmark, without the necessity to perform a large number of experimental tests. The force model allows to generate different sets of force data without the need of expensive experimental tests and without the influence of external noise on forces evaluation. The FE simulation methods are complementary to the analytical model because the simulations easily provide additional outputs and predictions such as surface integrity, burrs formation, and stress distributions on the tool [26, 27].

Machining includes a vast number of processes characterized by different tool geometries, workpiece-tool interaction and sizes. In particular, the size strongly affects the process modelling. The micro machining modelling is a complicated procedure due to the non-negligible elastic deformation, the tool run-out effect and the material behaviour discontinuity. Moreover, the chip fracture occurs at high and variable strain rates [8], in a field characterized by a relevant lack of material flow stress data. Srinivasa and Shunmugam [28] adapted a classic macro-end milling mechanistic model by considering the material strengthening and the edge radius effects. The comparison between the model prediction and the experimental data revealed an error ranging between 10 and 20%. Attanasio et al. [29] elaborated and calibrated an analytical model with the purpose of predicting the force components in slot micro milling. The tool run-out effect on the cutting edges trajectories was considered and a good matching with the experimental data was achieved. Moges et al. [30] developed a flexible force model by considering the effect of tool deflection on cutting forces. The phenomena substantially modified the tool flutes trajectories in micro machining with a considerable effect on the surface error variation in the tool axial direction.

When considering micro milling operations, a suitable force model should not neglect the presence of different cutting conditions, depending on actual uncut chip thickness. As reported in literature [31], two subsequent stages can be detected during micro-cutting, and different cutting modes are present in each stage. If the uncut chip thickness is lower than the Minimum Uncut Chip Thickness (MUCT), the dominated deformation regime is known as ploughing. In this condition, a ridge of material is deformed and pushed ahead of tool cutting edge without chip formation. If the uncut chip thickness overcomes the minimum uncut chip thickness, the cutting becomes a shearing-dominated process. Figure 1 illustrates the configuration of the slot micro milling operation. The uncut chip thickness t_u ranges from zero to a maximum value equal to the feed per tooth f_z for each flute and each rotation. The ploughing phenomena inevitably characterized the micro slot cutting, regardless of process parameters. The transition to the shearing regime occurs only if the feed per tooth is greater than the MUCT. Moreover, also in this condition, the ploughing affects the process for actual chip thickness ranging between zero and the MUCT value.

Vogler et al. [32] proposed the first effort to integrate the transition of cutting regimes in a micro milling analytical

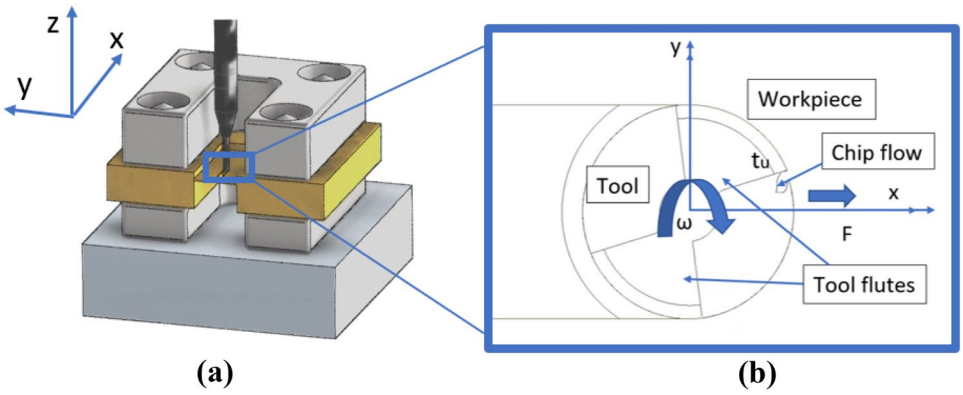

Fig. 1 Slot micro machining schematization: **a** three-dimensional representation, **b** two-dimensional detailed view

model. A slip-line force model was implemented to predict the cutting force when the chip thickness is greater than the minimum uncut chip thickness; in addition, an elastic deformation force model was employed when the chip thickness is smaller than the minimum uncut chip thickness. Since then, numerous force models which consider the presence of ploughing and shearing conditions have been elaborated. Rodriguez and Labarga [33] proposed an analytical force model by considering the run-out eccentric deviation, the tool deflection and the size effect. The model was expressed through a set of linear equations which considered the MUCT in order to define the entry and the exit angles of the milling tool in the workpiece. Malekian et at. [14] developed a ploughing force model which calculates the effect of elastic recovery by considering the interference volume between the tool and the workpiece. A conventional mechanistic model was implemented to calculate the shearing cutting force. The ploughing-shearing transition was identified with the purpose of understanding when each model should be used during the tool flute path. Chen et al. [34] proposed an analytical model that alternatively considers ploughing or shearing cutting conditions depending on the value of uncut chip thickness. The model calculates the instantaneous uncut chip thickness by considering the tool run-out and the machine tool system vibrations. Several experimental tests confirm that the model provides more accurate cutting force prediction than conventional models. Zhang et al. [35] elaborated a similar model which was validated by performing a series of micro end milling experiments on Al6061 workpieces under different cutting conditions.

3 Analytical force model development and refinement

This paper provides an analytical force model that is capable of predicting the cutting force by considering both ploughing and shearing regimes. The transition behaviour in cutting regime is identified through some preliminary tests. Once the MUCT is experimentally identified, it must be used as one of the model inputs. A detailed procedure to calculate the model parameters is subsequently described. The analytical model was finally employed to predict the cutting force during micro machining of Inconel 625 superalloy. This section provides a detailed description of the analytical model's structure. The mechanistic-based force model is suitable to predict the cutting force for slot micro milling. A two-dimensional micro milling of slots on thin-wall structure was considered as a reference configuration. The geometrical model corresponds with the experimental set-up. A 2-flutes, zero-degree rake angle and zero-degree helix angle end-mill was employed to perform the milling tests. The tool deflection was considered neglectable due to the stiffness of the tool compared with the intensity of the cutting forces.

In accordance with this hypothesis, the interaction between the tool cutting edge and the workpiece at a specific uncut chip thickness t_u determines the cutting force F_c. As showed in Fig. 2, F_c can be decomposed in the tangential component (F_t) and the radial component (F_r).

Furthermore, the resultant force can be decomposed in X–Y reference system as the sum of F_x and F_y components. In the proposed model the tangential and radial components of cutting forces can be computed as function of the actual tool rotation angle θ.

The angle θ depends on time t as expressed by the Eq. (1):

$$\theta(t) = \omega * t \tag{1}$$

At steady state, the first contact between tool and workpiece occurs when the tool rotation angle θ is equal to zero and the cutting edge is aligned along Y axis. Specific force parameters K_{ts} and K_{rs} are the shearing force coefficients in tangential and radial directions (N/mm^2) respectively, while parameters K_{tp} and K_{rp} are the ploughing force coefficients in tangential and radial directions (N/mm^3). The force coefficient values depend on the material properties and they should be determined through a refinement procedure. The cutting force components F_t and F_r can be computed through Eqs. (2) and (3):

$$F_t(\theta) = \left(K_{ts} * t_u(\theta) + K_{tp} * A_p(\theta)\right) * ADOC \tag{2}$$

$$F_r(\theta) = \left(K_{rs} * t_u(\theta) + K_{rp} * A_p(\theta)\right) * ADOC \tag{3}$$

The coefficient t_u is the actual uncut chip thickness while A_p is ploughed area while the parameter $ADOC$ is the axial depth of cut and it is equal to the thin wall

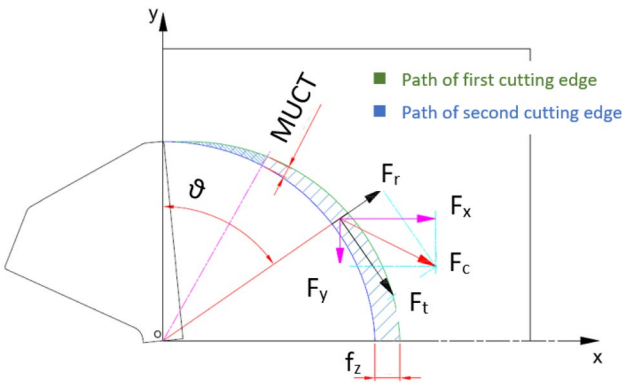

Fig. 2 Representation of MUCT, cutting area and cutting force decomposition

thickness. F_x and F_y components can be calculated from F_t and F_r by means of simple trigonometrical calculations, as shown by Eqs. (4) and (5):

$$F_x = F_t * \cos(\theta) + F_r * \sin(\theta) \quad (4)$$

$$F_y = -F_t * \sin(\theta) + F_r * \cos(\theta) \quad (5)$$

Figure 3 shows how the uncut chip thickness changed during a tool rotation while Fig. 4 shows how the ploughed area changed during a tool rotation. With the assumption of neglectable tool run-out, the thickness t_u ranges between zero and a maximum value, which is equal to feed per tooth f_z. The actual value of t_u can be computed as a function of the angle θ, as shown in Eq. (6) under the assumption that the tool run-out is negligible

$$t_u(\theta) = f_z * \sin(\omega * t) = f_z * \sin(\theta) \quad (6)$$

The ploughed area A_p is calculated as the area spanned by the tool cutting edge until t_u reaches the MUCT. When t_u becomes higher than the MUCT, A_p is kept constant until t_u decreases to the MUCT again. In the final portion of the cut, A_p decreases down to zero as cutting edge disengages from the workpiece material. The contribution of ploughing effect in the central portion of cut area (i.e. when t_u is higher than MUCT) is constant. The ploughed area A_p was calculated as the portion of the cutting area A_c which remain in the elastic deformation field. The cutting area A_c is defined as the amount of the material removed by a tool flute from 0° to θ, as expressed by the Eq. (7):

$$A_c(\theta) = \int_0^{\theta} \left(\frac{t_u(\theta) + t_u(\theta + d\theta)}{2} \right) R d\theta \quad (7)$$

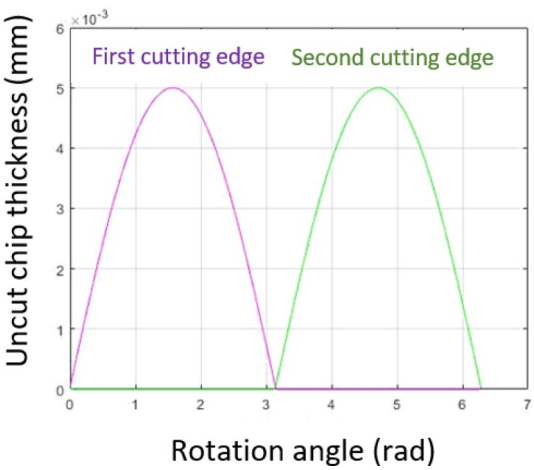

Fig. 3 Trend of uncut chip thickness (t_u) vs rotation angle (θ)

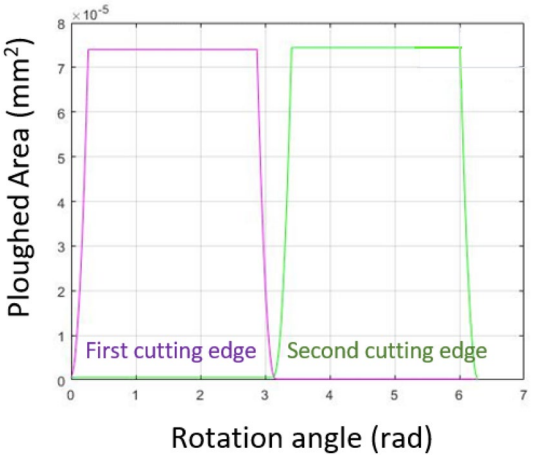

Fig. 4 Trend of ploughed area (A_p) vs rotation angle (θ)

The variable R indicates the tool radius as the half of the micro mill diameter. The Fig. 5 offers a representation of the cutting area $Ac(\theta)$. Once $Ac(\theta)$ is calculated, the Eq. set (8) can be used to compute A_p:

$$\text{Eq.set} \begin{cases} if t_u(\theta) < MUCT and \theta < \theta_{max} then A_p(\theta) = A_c(\theta) \\ if t_u(\theta) \langle MUCT and \theta \rangle \theta_{max} then A_p(\theta) = A_c(\pi) - A_c(\theta) \\ if t_u(\theta) > MUCT then A_p(\theta) = A_{pMAX} \end{cases} \quad (8)$$

The geometrical model does not consider the effect of tool run-out. The aim of the model is to predict the cutting force as a function of the material properties, without including the influence of external effects such as the tool run-out. The calibration procedure consists in two main phases.

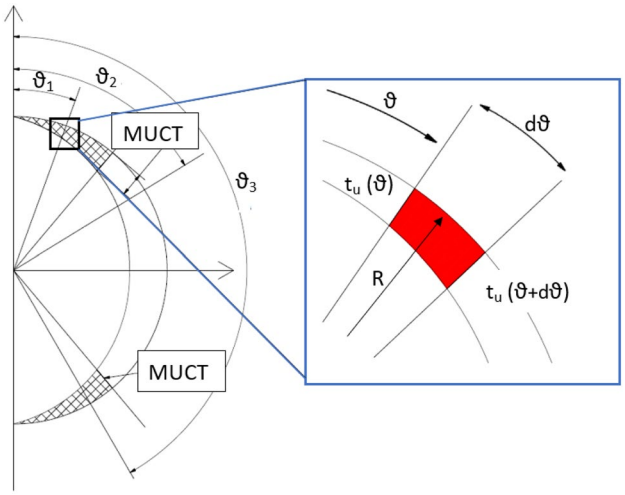

Fig. 5 A schematics of three possible positions of the tool cutting edge (θ_1, θ_2 and θ_3) with a detailed view of the infinitesimal cutting area (red coloured)

The first step is finalized to identify the MUCT while the second phase is designed to identify the analytical model coefficient K_{ts}, K_{rs}, K_{tp} and K_{rp}. The minimum uncut chip thickness can be experimentally determined by fabricating several channels on a sample by using a constant cutting speed and different feed per tooth (f_z) values. The cutting force normalization is performed through the Eq. 9, where $F_{cn}(\theta)$ is the Specific Cutting Force (SCF):

$$F_{cn}(\theta) = \frac{Fc(\theta)}{doc * t_u(\theta)} \tag{9}$$

The MUCT can be identified by considering the SCF as a function of the feed per tooth. Figure 6 shows an example of the typical trend of the SCF in micro milling wrought materials. It shows meaningful increments of the specific cutting force when the feed per tooth decreases. At low feed per tooth the transition between ploughing and shearing does not occur. The unique material remove mechanism is ploughing in this case and consequently it determines a pronounced specific cutting force increase compared to the test performed with higher feed rates. Therefore, the MUCT is equal to the feed per tooth value that is related to the change of the specific cutting force function. The second phase of the model refinement procedure consists of finding the optimal parameter set for the analytical force model. The purpose is to best fit the experimental cutting force data by minimizing the prediction error of the model.

Figure 7 shows an example of the cutting force components (F_x, F_y) and the resultant cutting force F_c. The force trends are representing the micro milling of a thin-walled sample that was described as a reference system given in Fig. 2. The F_z component is neglectable due to the tool helix angle, which is equal to zero degrees. The model considers tools with two flutes, indicated as cutting edge 1 (*CE1*) and cutting edge 2 (*CE2*). F_x, F_y and F_c show two peaks for a single tool round due to the tool run-out effect. Each peak could be associated with one of the two flutes. Moreover, the analytical model does not consider tool run-out and it provides two identical force peaks. The model refinement was performed through an iterative method. It was adopted by implementing a search algorithm. Several set of values must be tested until the minimum of an objective function is found. The objective function is defined as the difference between the cutting forces provided by the analytical model and the forces measured during the experimental tests. The implemented optimization algorithm is the Particle Swarm Optimization (PSO) by Eberhart and Kennedy [36], which was used in other researches related to the optimization of analytical model parameters as well as optimization of process parameters in different applications [37, 38].

An objective function which estimates the error as the difference between the average force peaks and the analytical model peak was defined. The average experimental F_x and F_y peaks are computed by the Eqs. 10 and 11. The error for F_x and F_y components is calculated through Eqs. 12 and 13. The Eq. 14 can be used to calculate the total error as the sum of the error for F_x and the error for F_y.

$$\overline{F_X(peak)} = \frac{F_{xmax}(CE1) + F_{xmax}(CE2)}{2} \tag{10}$$

$$\overline{F_y(peak)} = \frac{F_y\max(CE1) + F_y\max(CE2)}{2} \tag{11}$$

$$E_x = \overline{F_X(peak)} - F_{Xmodel}(peak) \tag{12}$$

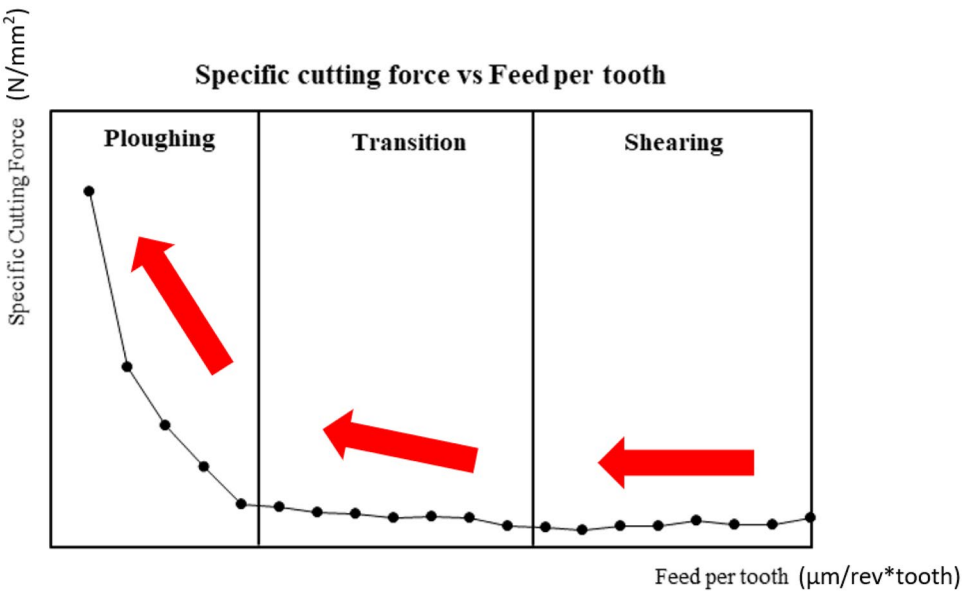

Fig. 6 An example of the specific cutting force peak as function of the feed per tooth for conventionally formed materials

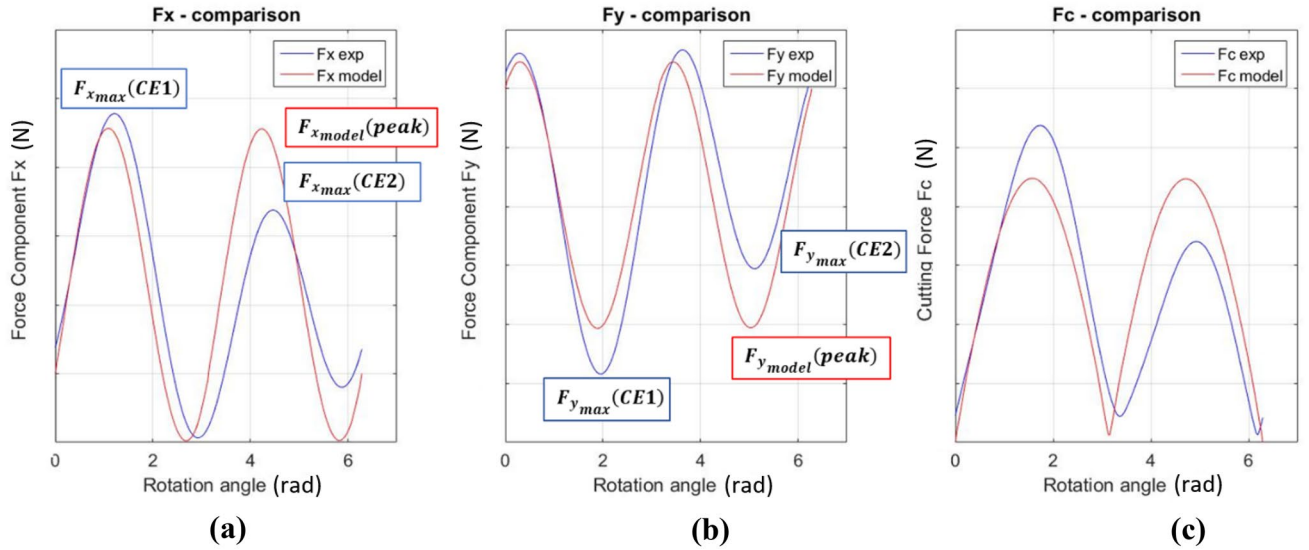

Fig. 7 An example of comparison between the experimental signal and the model prediction for the force component F_x (**a**); F_y (**b**) and the resultant cutting force F_c (**c**)

$$E_y = \overline{F_y(peak)} - F_{ymodel}(peak) \tag{13}$$

$$Err = \left|E_X\right| + \left|E_y\right| \tag{14}$$

The algorithm is based on the definition of a population of particles in a space with a dimension equal to the number n of the function parameters which must be optimized. Each particle is a n-dimensional vector and it represents a possible problem solution. For each particle, the algorithm calculates the objective function and it memorizes the results before changing the function parameters. The particles can be moved in a limited portion of the n-dimensional space defined through some parameters bounds. The geometrical and the analytical models were integrated in a Matlab function which calculates the cutting force components, the resultant and the error through Eqs. 1–14. In particular, the error Err was used as the algorithm objective function. The algorithm begins to compute the analytical cutting force by assuming some initial sets of model parameters K_{ts}, K_{rs}, K_{tp} and K_{rp} and it calculates the error by using the experimental data. Moreover, the algorithm iteratively changes the model coefficients by overwriting the particles' vector components. The particles variation is not arbitrary, and it was controlled through an algorithm set-up.

The inertial factor ω influences the maintenance of the particle direction between two consecutive iterations, enabling a control of the movement freedom. The particle movement is influenced by its own current position and by the global position of the swarm. A cognitive parameter C_1 and a social parameter C_2 are the weights respective of the current particle position and the swarm position. The Particle Swarm Optimization algorithm requires the experimental cutting force data as benchmark. The next section describes the experimental procedure to achieve this required benchmark data.

4 Materials and methods

The analytical model refinement and validation were performed through the execution of several micro milling tests. The tests can be divided in two categories: the micro slots at different feed rate to determine the MUCT and the thin-walled samples milling to calibrate the analytical model coefficient K_{ts}, K_{rs}, K_{tp} and K_{rp}. In each case, the tests were executed on Inconel 625 samples fabricated via L-PBF process with the same AM machine (GE Additive Concept Laser M2 Cusing) and process parameters. The laser power P, the scan velocity v_s, the laser spot size d, the laser thickness s, the hatch distance h, the stripe width w and volumetric energy density E are listed in Table 1.

The procedure can be performed on other material classes, such as steel, brass and titanium alloys. Table 2 summarizes the chemical composition of the certified Inconel 625 provided by the supplier, while Table 3 shows the mechanical properties of this material "as-built" in Z

Table 1 AM process parameters

P (W)	v_s (mm/s)	d (μm)	s (μm)	h (μm)	w (mm)	E (J/mm^3)
370	1200	170	60	110	5	46.7

Table 2 Chemical composition of Inconel 625

	Ni	Cr	Mo	Cb	Fe	Si	Al	Ti
Wt (%)	61.6	22.0	9.0	4.0	3.0	< 0.3	< 0.2	< 0.2

Table 3 Mechanical properties of Inconel 625 [39]

Specimen orientation (X, Y, Z)	Yield strength (MPa)	Ultimate tensile strength (MPa)	Elongation (%)	Hardness (HRC)
Z	410	750	44	14

direction. The powder particle size was ranging between 15 µm and 45 µm. The samples were not heat treated (or hot isostatically pressed).

Figure 8 shows the geometry of the sample utilized for the test finalized to the MUCT identification (Fig. 8a) and the geometry of the thin-walled sample used to calibrate the analytical model coefficients (Fig. 8b). Both experimental procedures were performed by using a 5-axis nano-precision milling center (Kern Pyramid Nano) equipped with a cutting force measurement system. The machining was performed in dry condition, without using cooling lubricant. The loads generated by the interaction between tool and workpiece must be measured by using an adequate force measurement and acquisition system. The load acquisition system consists of a piezoelectric 3-component force sensor (Kistler 9317C) interfaced to three charge amplifiers (Kistler 5015A) which produce amplified voltage signals as output. The sample shapes were designed in order to constrain the samples on the loadcell. The force measuring system accuracy is equal to 0.1 N, the sampling rate is 50 kHz and the natural frequency is lower than the tooth path frequency [40].

4.1 MUCT micro milling test

The machining tests consist in the fabrication of twenty channels by using a constant cutting speed and twenty different feed per tooth f_z values, ranging between 0.5 µm/rev × tooth and 10 µm/rev × tooth. The channels were fabricated on a flat surface which was obtained through a face milling operation. The surface roughing was performed by using a two-flute carbide end-mill with a diameter of 6 mm. A cutting speed of 54 m/min, a feed rate of 50 mm/min and an axial depth of cut *ADOC* of 0.2 mm were utilized to execute the rough machining. All slots were machined by using a two-flute micro mill under the same run-out condition. The cutting speed was set at 40 m/min and the depth of cut was fixed at 200 µm, as suggested by the tool manufacturer for hard-to-cut non-ferrous material. The actual tool geometry was acquired and checked by using a 3D digital microscope (Hirox RH 2000). Table 4 presents further details about the micro end mill.

Five consecutive slots were fabricated on each side of the sample. The length of the slots kept constant as 8 mm. Between two consecutive cuts, the tool flutes were cleaned to remove sticking material and to avoid the build-up edge phenomena. A feed per tooth increment of 0.5 µm was adopted between two consecutive slot machining, from a minimum f_z equal to 0.5 µm/rev × tooth to a maximum of 10 µm/rev × tooth. Any feed per tooth value lower than the MUCT does not allow the transition from the ploughing to the shearing regime.

The cutting force components were acquired with the loadcell during the whole channel fabrication. The resultant cutting

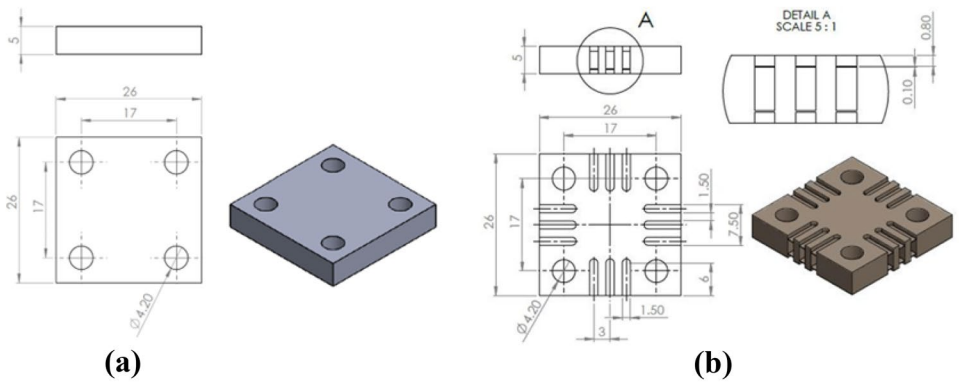

Fig. 8 The workpiece geometries: **a** for the MUCT test, **b** for the thin-wall cuts

Table 4 Micro end mill features

Feature	Value
Manufacturer	SECO
Model code	SECO905L008-MEGA-T
Nominal diameter (μm)	800
Effective diameter (μm)	791 ± 1
Nominal cutting edge radius (μm)	5
Helix angle (°)	20
Rake angle (°)	4
Material	Tungsten Carbide
Material coating	Titanium Nitride

force was obtained and smoothed by using a low-pass filter with a cut-off frequency of 1000 Hz. The maximum peaks of the cutting force were not modified by the filter because the tooth passing frequency is lower than the cut-off frequency. The tooth passing frequency can be calculated by using Eq. 15 and it is equal to 530 Hz.

$$f_{TP} = \frac{n}{60} * z \tag{15}$$

Therefore, the slots fabricated at minimum feed rate are characterized by higher than usual specific cutting force due to the uncorrected deformation regime. During each test the cutting force components were measured, and they were subsequently composed to calculate the resultant cutting force F_c for each time instant. The cutting force strongly depends on the chip cross-section S. Equation 16 allows to calculate the chip cross-section as the product between the axial depth of cut $ADOC$ and the chip thickness t_u.

$$S = ADOC * t_u \tag{16}$$

In slot micro milling the chip thickness t_u can be calculated as a function of the flute rotation angle ωt as expressed by the Eq. 17.

$$t_u = f_z * \sin(\omega t) \tag{17}$$

The cutting force F_c oscillates between a minimum value and a maximum peak F_{C_Max} during a tool rotation of 180°. Moreover, the maximum load F_{C_Max} corresponds to the maximum cross-section equal to the product between the axial depth of cut ($ADOC$) and the feed per tooth (f_z). The decrease of f_z between two consecutive test determines a section (S) reduction which has a considerable effect on the cutting force value. To highlight the dependence of the cutting force in relation to the deformation mechanism, the specific cutting force must be calculated by Eq. 18:

$$F_{C\_Max\_n} = \frac{F_{C\_Max}}{S} \tag{18}$$

Table 5 Zero-degree helix angle micro end mill features

Feature	**Value**
Manufacturer	SECO
Model code	103L008R005-MEGA-64T
Nominal (μm)	800
Effective diameter (μm)	789 ± 3
Nominal cutting edge radius (μm)	4
Helix angle (°)	0
Material	Tungsten Carbide
Material coating	Titanium Nitride

4.2 Thin-wall micro milling test

Once the MUCT is determined, some orthogonal cutting tests must be performed to calculate the analytical model parameters. Experimental tests have been carried out assuming a thin-wall channel-milling configuration. The thin-wall configuration, as well as the use of end-mill tools with 0° helix angle, has been assumed in order to replicate orthogonal cutting conditions [41]. The thin wall was fabricated via Additive Manufacturing with a nominal thickness of 0.2 mm. The actual thin wall thickness was measured by using the 3D multifocal microscope Hirox RH 2000. The actual thickness value corresponds to the depth of cut ($ADOC$). Table 5 presents further details about the zero-degree helix micro end mill used in actual thin-wall milling tests.

The analytical force model allows to compute cutting forces as a function of uncut chip thickness by considering the presence of different cutting regimes. The refined analytical force model will be used for the generating force data under different cutting conditions. Therefore, a validation procedure was performed by machining several samples with different combinations of feed per tooth and cutting speed. The machining tests consist in the fabrication of a through-channel for each thin-wall. Three feed per tooth values (2.5, 5, and 10 μm/rev × tooth) and two cutting speeds (30, 40 m/min) were combined while the channel length was set constant and equal to 5 mm. Each test was repeated three times to statistically validate the analytical model. During the machining, the load measurement system was utilized to acquire the cutting force F_c. A uniform portion corresponding to thirty tool rotations was considered for each test, and an average cutting force signal was finally computed for each slot fabrication.

Table 6 summarized the process parameters combinations. The depth of cut was identified by measuring the thickness of the thin-wall before performing the cutting test. The measurements were executed with five repetition along each thin wall by using the microscope Hirox RH-2000 and the average thickness was found to be 171 ± 17 μm. Table 7 summarized the actual thickness

Table 6 Process parameters combinations

Test	Cutting speed (m/min)	Feed per tooth (μm/rev × tooth)
A	30	2.5
B	40	2.5
C	30	5
D	40	5
E	30	10
F	40	10

Table 7 Process parameters and samples actual dimensions

Test	Actual thickness (μm)	Deviation (μm)	Test	Actual thickness (μm)	Deviation (μm)
A1	171 ± 2	29	D2	176 ± 4	24
B1	180 ± 2	20	E2	177 ± 4	23
C1	200 ± 3	0	F2	199 ± 2	1
D1	174 ± 3	26	A3	168 ± 2	32
E1	150 ± 2	50	B3	178 ± 1	22
F1	137 ± 3	63	C3	175 ± 3	25
A2	154 ± 3	46	D3	186 ± 2	14
B2	165 ± 2	32	E3	187 ± 1	13
C2	155 ± 3	45	F3	149 ± 2	51

with the standard deviation and the deviation from the nominal value of 200 μm. The results highlight on one hand a uniform thickness along each thin wall, moreover the thickness differ from one another by a non-negligible quantity. For this reason, the effective thickness of each thin-wall was utilized in the analytical model calibration and validation instead of the average value.

5 Results and discussion

Twenty slots were fabricated on an Inconel 625 sample with the purpose of identifying MUCT. A central portion of the filtered signal corresponding to thirty tool rotations was extrapolated. During the cut, the force signal exhibits a variability and a single tool rotation can not be considered. Moreover, for each rotation and for each flute the maximum cutting force peak was computed. The average cutting force peaks between the two flutes was calculated for each rotation and finally an average maximum cutting force was computed for each slot. The standard deviation of the average cutting force was calculated by considering the maximum cutting force for each of the thirty tool rotations. The cutting forces were normalized by using Eq. 18 to eliminate the influence of the chip cross section. The numerical results and the relation between the specific cutting force and the feed per tooth is visible in Fig. 9.

The specific cutting force is not constant, and it decreases as the feed rate decreases. The results are qualitatively comparable with the trend of conventional fabricated workpiece [42]. For feed per tooth higher than 6 μm, the specific cutting force is almost constant. During the tests performed with the highest feed rate, the transition from ploughing to shearing regime occurs when the tool rotation angle θ is nearly zero. In shearing dominant zone, the ploughing effect cannot affect the cutting force peak. The tests performed with feed per tooth lower than 2.5 μm are characterized by the presence of a single cutting regime, hence the ploughing. The average force peak increases as the feed rate decreases. When ploughing is the dominant regime, the cutting process becomes instable due to the unaccounted material removal behaviour. Maximum F_c are more variable as demonstrated by a larger standard deviation of the data, visible as the error bars in the graph of Fig. 9b. During the transition between

n	f_z (μm/rev*tooth)	Fc_n (N/mm²)	*n*	f_z (μm/rev*tooth)	Fc_n (N/mm²)
1	10	13354.9	**11**	5	21405.3
2	9.5	11466.1	**12**	4.5	23145.3
3	9	12057.0	**13**	4	24285.3
4	8.5	13626.0	**14**	3.5	26631.2
5	8	13736.9	**15**	3	29045.6
6	7.5	15096.9	**16**	2.5	35357.0
7	7	16142.6	**17**	2	36210.1
8	6.5	15345.3	**18**	1.5	45648.43
9	6	16238.0	**19**	1	69289.2
10	5.5	17543.9	**20**	0.5	112590.9

(a)

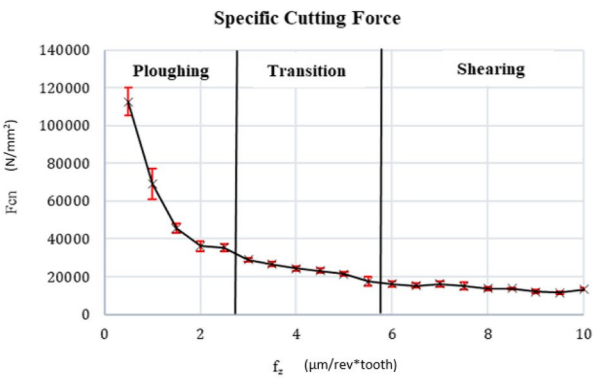

(b)

Fig. 9 The average maximum specific cutting force (**a**) and the correlation between the maximum specific cutting force and the feed per tooth (**b**

ploughing and shearing, the correlation between specific cutting force and feed per tooth is linear. The minimum uncut chip thickness was identified as the feed per tooth value corresponding to the beginning of the ploughing dominant zone. Therefore, the value of the MUCT was set equal to 2.5 µm. This value was employed in the analytical force model algorithm for the refinement procedure.

The procedure requires measured cutting force data during the test performed on the micro milling of thin walls. A portion of the signal (corresponding to thirty tool rotation) was extrapolated and it was utilized to calculate the average value and the standard deviation of the data for each tool rotation angle θ. Figure 10 shows the average cutting force, with lower and upper bounds, measured during the thin wall machining executed with a cutting speed of 30 m/min at different feed per tooth f_Z. Tests A (Fig. 10a), C (Fig. 10b) and E (Fig. 10c) are characterized by increasing feed per tooth, from 2.5 to 10 µm/rev × tooth.

The tool run-out determines unbalanced cutting condition between the flutes, but it is clear that cutting force peaks increase as the feed rate increases. The tests performed with a cutting speed of 40 m/min show an analogue trend (Test B, D, F). Table 8 summarizes the average cutting force peak for each cutting edge (*Fc CE1* and *Fc CE2*) and the ratio between peaks. The ratio between the cutting force peaks on the flutes is equal to 1.5 for Test E1, while the ratio for Test A1 is equal to 3.2 and for Test C1 is equal to 1.9. The load unbalance between the tool flutes is higher at low feed rate where the ploughing effects are more relevant. For that reason, the feed per tooth $f_z = 10$ µm/rev × tooth was identified as optimal for the cutting model calibration.

The highest f_z combined with a cutting speed of 30 m/min allows minimizing tool run-out effects and consequently reducing the approximation about the model parameters calculation. Therefore, the more reliable model calibration was executed by using the experimental data measured during Tests E. The machining test performed in different conditions were utilized to provide the analytical model validation by comparing the model prevision with the experimental data.

Table 8 Average peaks of the cutting force for each tool flute and their ratio

Test	f_z (µm/rev/tooth)	F_c CE1 (N)	F_c CE2 (N)	F_c CE1/F_c CE2
A1	2.5	3.43	1.06	3.2
C1	5	5.21	2.73	1.9
E1	10	6.08	4.05	1.5

The refinement of the analytical force model was performed by using the Particle Swarm Optimization, an optimization algorithm for continuous non-linear function. After several trial optimizations, the cognitive parameter C_1 and the social parameter C_2 were set at 1.2 and 0.012, while the inertial factor W was set at 0.0004. The number of particles and iterations were defined as a trade-off between the error minimization and the computational time. A stable solution was found by the algorithm after 1000 iterations with 150 particles. Table 9 summarizes the model coefficient bounds. The bounds were changed until the particles did not find the optimal solution in correspondence of their limits. The last column of Table 9 reports the result of the optimization procedure.

The calibrated analytical force model was utilized to predict the cutting force F_c for all the combinations of cutting speed, feed per tooth and thickness summarized in Table 7. The comparison between the model predictions and the experimental forces allowed to validate the analytical force model refinement. The most important term of comparison is certainly the cutting force peaks. A correct prediction of the maximum force during the process allows estimating the

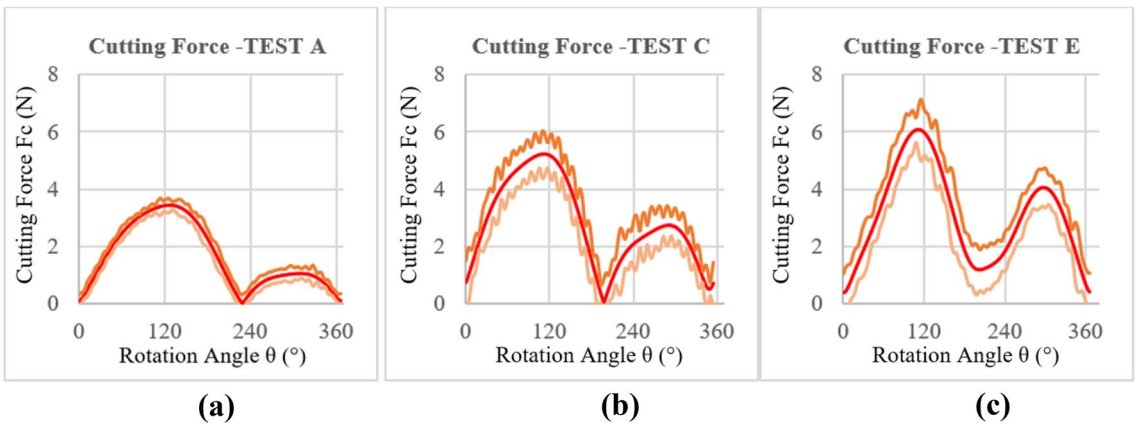

Fig. 10 Average cutting force with lower and upper bounds for Test A1 (**a**), Test C1 (**b**) and Test E1 (**c**)

Table 9 Lower and upper limits and optimum set of the analytical force model coefficient

Parameter	Lower Bound	Upper Bound	Optimum set
K_{ts}	0	10,000	2595
K_{tp}	0	5000	4625
K_{rs}	0	10,000	1870
K_{rp}	0	5000	3000

maximum bending force of the tool and predicting a possible failure in the micro-end mill. The experimental cutting force and the analytical force model peaks are listed in Table 10. The maximum value of the experimental cutting force was calculated as the average value between the two cutting edge force peaks. The last column expresses the percentage error about the prediction. The model provided accurate results, since the error ranged between 0.8% and 14.6%. The prediction of the cutting force peaks is acceptable regardless the dominant material removing behavior. In fact, the percentage error is low for the tests performed in a shearing dominant condition ($f_z = 10$ µm/rev × tooth), during the material behaviour transition ($f_z = 5$ µm/rev × tooth) and also when the ploughing regime is dominant ($f_z = 2.5$ µm/rev × tooth).

The analytical force model can be employed also to verify the accuracy of the MUCT identification procedure. In fact, the analytical force model was also utilized to predict the experimental cutting force with different MUCT values, in particular with MUCT' = 2 µm and MUCT'' = 1.5 µm. The prediction error increased compared to the errors achieved with MUCT = 2.5 µm. The average error increment was equal to 22% with MUCT' and 64% with MUCT''.

Figure 11 shows the comparison for the Tests A and Tests B. The experimental limits were built by adding or subtracting the average value with the standard deviation. The tool run-out strongly affects the experimental data since it is comparable with the feed per tooth. The deviation of the tool trajectories determines a meaningful difference between the two peaks and between the periods of engagement of the tool flutes. The analytical force model does not consider this imbalance, which has a significant role in ploughing regime also due to the formation of build-up edge material accumulation on the tool flute. Each test was repeated three times and the analytical model prediction was calculated by considering the effective thickness of the samples. The average percentage error for each combination of the process parameters was calculated. The results are visible in Table 11.

The best model prediction occurs when the cutting dominant mode is shearing. The average error for Tests E is − 1.7% while for Tests F is − 0.9%. The imbalance between the tool cutting edges is almost negligible, as visible in Fig. 10c. The advantageous experimental condition allowed to calculate the average cutting force between the tool flutes for the entire signal, and not only for the peaks as made for the test in ploughing regime.

However, the model offers a very accurate prediction of the cutting load peaks in ploughing dominant regime since the error is equal to − 2.5% for Tests A and − 1.9% for Tests B. During the transition between shearing and ploughing the prediction is less accurate since that the tests performed with feed per tooth equal to 5 µm/rev × tooth exhibit the highest error. The error on peaks is 10.4% for Tests C and 12.4% for Tests D. The model is less reliable than ploughing and shearing dominant regime. Moreover, also in transition zone the prediction was considered enough accurate considering the variability of micro milling process, which is strongly influenced by numerous factors.

Figure 12 shows the comparison between two tests with same cutting speed and different feed per tooth. Tests C (Fig. 12a) shows an example of prediction in transition zone while Tests E (Fig. 12b) considers the shearing dominant zone. An analogue trend was obtained at higher cutting speed for Tests D and Tests F. The analytical force model provides an accurate cutting force prevision since

Table 10 The average peak of the experimental cutting force and the analytical model prediction

Test	Fc MAX experimental (N)	Fc MAX analytical model (N)	Error (%)	Test	Fc MAX experimental (N)	Fc MAX analytical model (N)	Error (%)
A1	2.24	2.28	– 1.7	D2	3.51	3.06	12.8
B1	2.37	2.43	– 2.3	E2	5.60	5.83	– 4.1
C1	3.97	3.48	12.7	F2	6.29	6.48	– 3.0
D1	3.35	3.02	9.9	A3	2.21	2.25	– 1.8
E1	5.07	4.92	3.0	B3	2.36	2.38	– 0.8
F1	4.39	4.47	– 1.9	C3	3.30	3.04	7.9
A2	1.98	2.06	– 4.0	D3	3.78	3.23	14.6
B2	2.16	2.21	– 2.3	E3	5.86	6.10	– 4.1
C2	3.02	2.69	10.9	F3	4.97	4.86	2.2

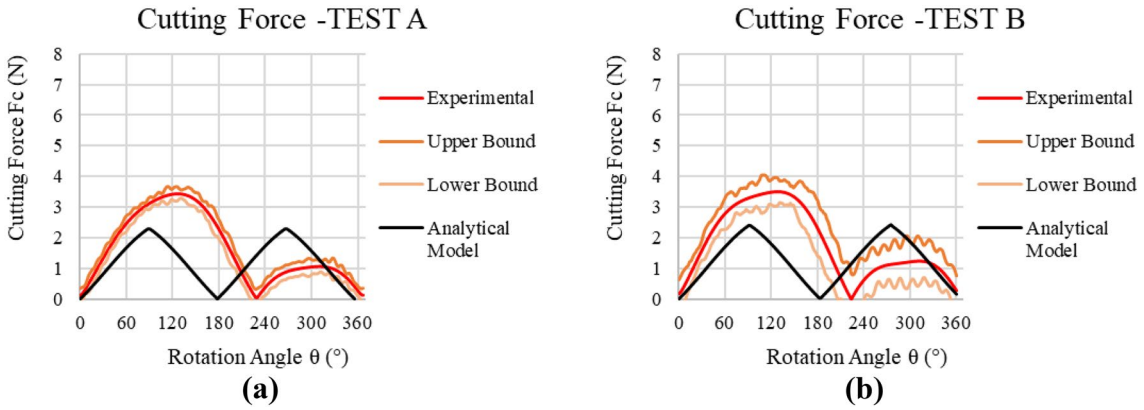

Fig. 11 Comparison between the experimental data and the model prediction for Test A1 (**a**) and Test B1 (**b**)

Table 11 Average error of the analytical model

Test	Cutting speed (m/min)	Feed per tooth (µm/rev × tooth)	Average Error (%)
A	30	2.5	– 2.5
B	40	2.5	– 1.9
C	30	5	10.4
D	40	5	12.4
E	30	10	– 1.7
F	40	10	– 0.9

that F_c is included between the experimental upper and lower limits. Moreover, the model is more powerful in shearing regime since the error about force peaks is minimum and the prediction is extremely accurate along the entire tool rotation.

6 Conclusions

This study presents formulation of an analytical force model for slot micro milling which considers the concurrent presence of different cutting regimes i.e. ploughing and shearing. This analytical model feature allows successfully applying the force model on a wide range of process parameters including and high feed rate cases. A model refinement procedure is described and applied on an experimental case, micro milling of an additive fabricated Inconel 625 superalloy where material behavior in cutting is considered as unknown. An accurate load measurement system provides collecting cutting force data useful for the model assessment. The experimental investigation of the cutting regimes transiting from shearing to ploughing allowed identifying a MUCT value that is equal to 2.5 µm. This parameter offers an important information about the machinability of the additively fabricated Inconel 625 superalloy and, at the same time, it covers a key role as an analytical model input. After the model refinement procedure, the model offers a

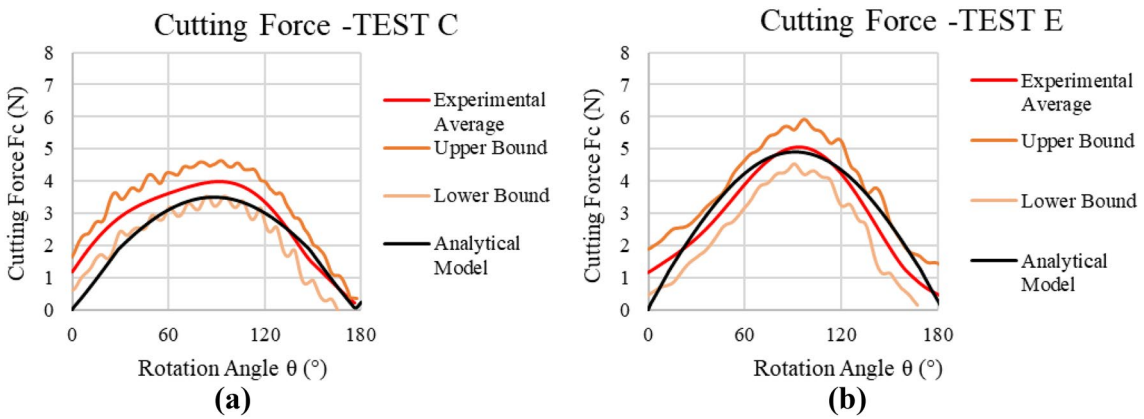

Fig. 12 Comparison between the experimental data and the model prediction for Test C1 (**a**) and Test E1 (**b**)

good prediction of the tangential and radial components of the cutting forces. The percentage error of the prediction is calculated for each test by considering the resultant cutting force. The proposed analytical force model offers reliable prediction in accord with the experimental data. The model will be further tested on a single flute tool to avoid the influence of tool run-out. The model refinement procedure will be performed on other difficult-to-cut materials.

References

1. Herzog D, Seyda V, Wycisk E, Emmelmann C (2016) Additive manufacturing of metals. Acta Mater 117:371–392
2. DebRoy T, Wei HL, Zuback JS, Mukherjee T, Elmer JW, Milewski JO, Beese AM, Wilson-Heid A, De A, Zhang W (2017) Additive manufacturing of metallic components—process, structure and properties. Prog Mater Sci 92:112–224
3. Ma M, Wang Z, Gao M, Zeng X (2014) Layer thickness dependence of performance in high-power selective laser melting of 1Cr18Ni9Ti stainless steel. J Mater Process Technol 215:142–150
4. Criales LE, Arisoy YM, Lane B, Moylan S, Donmez A, Özel T (2017) Laser powder bed fusion of nickel alloy 625: experimental investigations of effects of process parameters on melt pool size and shape with spatter analysis. Int J Mach Tools Manuf 121:22–36
5. Ford S, Despeisse M (2016) Additive manufacturing and sustainability: an exploratory study of the advantages and challenges. J Clean Prod 137:1573–1587
6. Özel T, Altay A, Donmez A, Leach R (2018) Surface topography investigations on nickel alloy 625 fabricated via laser powder bed fusion. Int J Adv Manuf Technol 94(9–12):4451–4458
7. Alting L, Kimura F, Hansen HN, Bissacco G (2003) Micro engineering. CIRP Ann Manuf Technol 52(2):635–657
8. Dornfeld D, Min S, Takeuchi Y (2006) Recent advances in mechanical micromachining. CIRP Ann Manuf Technol 55(2):745–768
9. Biermann D, Kahnis P (2010) Analysis and simulation of size effects in micromilling. Product Eng Res Dev 4(1):25–34
10. Chrzanowski W, Neel EAA, Armitage DA, Knowles JC (2008) Effect of surface treatment on the bioactivity of nickel-titanium. Acta Biomater 4(6):1969–1984
11. Trosch T, Strößner J, Völkl R, Glatzel U (2016) Microstructure and mechanical properties of selective laser melted Inconel 718 compared to forging and casting. Mater Lett 164(1):428–431
12. Sharman ARC, Hughes JI, Ridgway K (2006) Workpiece surface integrity and tool life issues when turning Inconel 718 nickel based superalloy. Mach Sci Technol 8(3):399–414
13. Patel K, Fei J, Liu G, Özel T (2019) Milling investigations and yield strength calculations for nickel alloy Inconel 625 manufactured with laser powder bed fusion process. Prod Eng 13(6):693–702
14. Malekian M, Park SS, Jun MBG (2009) Modelling of dynamic micro-milling cutting forces. Int J Mach Tools Manuf 49(7–8):586–598
15. Bissacco G, Hansen HN, Slunsky J (2008) Modelling the cutting edge radius size effect for force prediction in micro milling. CIRP Ann Manuf Technol 57(1):113–116
16. Shi Z, Li Y, Liu Z, Qiao Z (2018) Determination of minimum uncut chip thickness during micro-end milling Inconel 718 with acoustic emission signals and FEM simulation. Int J Adv Manuf Technol 98(1–4):37–45
17. Przestacki D, Chwalczuk T, Wojciechowski S (2017) The study on minimum uncut chip thickness and cutting forces during laser-assisted turning of WC/NiCr clad layers. Int J Adv Manuf Technol 91(9–12):3887–3898
18. Brandão F, Rodrigues AR, Coelho RT, Fagali A (2015) Size effect and minimum chip thickness in micromilling. Int J Mach Tools Manuf 89:39–54
19. Allegri G, Colpani A, Ginestra PS, Attanasio A (2019) An experimental study on micro-milling of a medical grade Co-Cr-Mo alloy produced by selective laser melting. Materials 12(13):1–12
20. Malekian M, Mostofa MG, Park SS, Jun MBG (2012) Modeling of minimum uncut chip thickness in micro machining of aluminum. J Mater Process Technol 212(3):553–559
21. Bao WY, Tansel IN (2000) Modeling micro-end-milling operations. Part I: analytical cutting force model. Int J Mach Tools Manuf 40:2155–2173
22. Zhou L, Peng FY, Yana R, Yao PF, Yang CC, Li B (2015) Analytical modeling and experimental validation of micro end-milling cutting forces considering edge radius and material strengthening effects. Int J Mach Tools Manuf 97:29–41
23. Zhang X, Ehmann KF, Yu T, Wang W (2016) Cutting forces in micro-end-milling processes. Int J Mach Tools Manuf 107:21–40
24. Shankar V, Bhanu Sankara Rao K, Mannan SL (2001) Microstructure and mechanical properties of Inconel 625 superalloy. J Nucl Mater 288:222–232
25. Özel T, Karpat Y (2007) Identification of constitutive material model parameters for high-strain rate metal cutting conditions using evolutionary computational algorithms. Mater Manuf Process 22:659–667
26. Özel T, Olleak A, Thepsonthi T (2017) Micro milling of titanium alloy Ti-6Al-4 V: 3-D finite element modeling for prediction of chip flow and burr formation. Prod Eng 11(4–5):435–444
27. Attanasio A, Abeni A, Ceretti E, Özel T (2019) Finite element simulation of high speed micro milling in the presence of tool run-out with experimental validations. Int J Adv Manuf Technol 100(1–4):25–35
28. Srinivasa YV, Shunmugam MS (2013) Mechanistic model for prediction of cutting forces in micro end-milling and experimental comparison. Int J Mach Tools Manuf 67:18–27
29. Attanasio A, Garbellini A, Ceretti E, Giardini C (2015) Force modelling in micromilling of channels. Int J Nanomanuf 11(5–6):275–296
30. Moges TM, Desai KA, Rao PVM (2018) Modeling of cutting force, tool deflection, and surface error in micro-milling operation. Int J Adv Manuf Technol 98(9–12):2865–2881
31. Gelfi M, Attanasio A, Ceretti E, Garbellini A, Pola A (2019) Micromilling of lamellar Ti6Al4V: cutting force analysis. Mater Manuf Process 31(7):919–925
32. Vogler MP, Kapoor SG, DeVor RE (2004) On the modeling and analysis of machining performance in micro end milling, part II: cutting force prediction. ASME J Manuf Sci Eng 126(4):695–705
33. Rodríguez P, Labarga JE (2013) A new model for the prediction of cutting forces in micro-end-milling operations. J Mater Process Technol 213:261–268
34. Chen W, Teng X, Huo D, Wang Q (2017) An improved cutting force model for micro milling considering machining dynamics. Int J Adv Manuf Technol 93(9–12):3005–3016
35. Zhang X, Yu T, Wang W (2018) Dynamic cutting force prediction for micro end milling considering tool vibrations and run-out. Proc Inst Mech Eng Part C J Mech Eng Sci 233(7):2248–2261
36. Eberhart R, Kennedy J (1995) A new optimizer using particle swarm theory. In: Proceedings of the Sixth International Symposium on IEEE. 1995:39-43
37. Raja SB, Baskar N (2011) Particle swarm optimization technique for determining optimal machining parameters of different work

piece materials in turning operation. Int J Adv Manuf Technol 54(5–8):445–463
38. Ciurana J, Arias G, Özel T (2009) Neural network modeling and particle swarm optimization (PSO) of process parameters in pulsed laser micromachining of hardened AISI H13 steel. Mater Manuf Process 24(3):358–368
39. Lewandowski JJ, Seifi M (2016) Metal additive manufacturing: a review of mechanical properties. Annu Rev Materi Res 46:151–186
40. Abeni A, Lancini M, Attanasio A (2019) Characterization of machine tools and measurement system for micromilling. Nanotechnol Precis Eng 2:23–28
41. Attanasio A, Abeni A, Özel T, Ceretti E (2018) Finite element simulation of high speed micro milling in the presence of tool run-out with experimental validations. Int J Adv Manuf Technol 100(1–4):25–35
42. Lai X, Li H, Li C, Lin Z, Ni J (2008) Modelling and analysis of micro scale milling considering size effect, micro cutter edge radius and minimum chip thickness. Int J Mach Tools Manuf 48(1):1–14